Exophilin8 transiently clusters insulin granules at the actin-rich cell cortex prior to exocytosis

Kouichi Mizuno[a], José S. Ramalho[b], and Tetsuro Izumi[a]
[a]Laboratory of Molecular Endocrinology and Metabolism, Department of Molecular Medicine, Institute for Molecular and Cellular Regulation, Gunma University, Maebashi 371–8512, Japan; [b]CEDOC, Faculty of Medical Sciences, NOVA University, 1169–056 Lisbon, Portugal

ABSTRACT **Exophilin8/MyRIP/Slac2-c is an effector protein of the small GTPase Rab27a and is specifically localized on retinal melanosomes and secretory granules. We investigated the role of exophilin8 in insulin granule trafficking. Exogenous expression of exophilin8 in pancreatic β cells or their cell line, MIN6, polarized (exophilin8-positive) insulin granules at the cell corners, where both cortical actin and the microtubule plus-end–binding protein, EB1, were present. Mutation analyses indicated that the ability of exophilin8 to act as a linker between Rab27a and myosin Va is essential for its granule-clustering activity. Moreover, exophilin8 and exophilin8-associated insulin granules were markedly stable and immobile. Total internal reflection fluorescence microscopy indicated that exophilin8 restricts the motion of insulin granules at a region deeper than that where another Rab27a effector, granuphilin, accumulates docked granules directly attached to the plasma membrane. However, the exophilin8-induced immobility of insulin granules was eliminated upon secretagogue stimulation and did not inhibit evoked exocytosis. Furthermore, exophilin8 depletion prevents insulin granules from being transported close to the plasma membrane and inhibits their fusion. These findings indicate that exophilin8 transiently traps insulin granules into the cortical actin network close to the microtubule plus-ends and supplies them for release during the stimulation.**

Monitoring Editor
David G. Drubin
Unversity of California, Berkeley

Received: May 7, 2010
Revised: Feb 9, 2011
Accepted: Mar 11, 2011

INTRODUCTION

Insulin release from pancreatic β cells plays an essential role in blood glucose homeostasis. Insulin-containing secretory granules are formed at the *trans*-Golgi network and transported close to the plasma membrane for subsequent exocytosis. Although the precise mechanism is unknown, granule transport to the cell periphery could involve cytoskeletal elements. Live cell imaging in neuroendocrine PC12 cells has revealed that newly formed immature secretory granules are transported in a microtubule-dependent manner within a few seconds to the cell periphery and are then restricted to the F-actin–rich cell cortex (Rudolf *et al.*, 2001). Kinesin-1 localized on secretory granules is proposed to mediate microtubule-based granule transport because exogenous expression of its motor domain carrying a mutation in the ATP-binding motif blocks fast and long-range granule movements in the pancreatic β-cell line INS-1 (Varadi *et al.*, 2002). Furthermore, an actin-based motor protein, myosin Va, may play a role in granule interaction with F-actin because expression of its C-terminal tail fragment lacking the motor domain inhibits cortical localization of granules and induces cluster formation in PC12 cells as well as the β-cell line MIN6 (Rudolf *et al.*, 2003; Varadi *et al.*, 2005). These findings suggest that newly formed granules are transferred from microtubules to the cortical F-actin network, although these dominant-negative types of experiments should not be considered conclusive.

The melanosomes in skin melanocytes provide an excellent example of rapid microtubule-dependent translocation and subsequent myosin Va–dependent interaction with a peripheral F-actin network (Wu *et al.*, 1998). The protein melanophilin links the small GTPase Rab27a on melanosomes with myosin Va on actin filaments (Fukuda *et al.*, 2002; Nagashima *et al.*, 2002; Strom *et al.*, 2002; Wu *et al.*, 2002). Without capture onto the actin network in the cell

This article was published online ahead of print in MBoC in Press (http://www.molbiolcell.org/cgi/doi/10.1091/mbc.E10-05-0404) on March 25, 2011.

Address correspondence to: T. Izumi (tizumi@showa.gunma-u.ac.jp).

Abbreviations used: cDNA, complementary DNA; EGFP, enhanced green fluorescent protein; EM-CCD, electron multiplying charge-coupled camera; FRAP, fluorescence recovery after photobleaching; GST, glutathione-*S*-transferase; HA, hemagglutinin; KO1, Kusabira-Orange 1; KRB, Krebs Ringer buffer; MSD, mean square displacement; NPY, neuropeptide Y; PBS, phosphate-buffered saline; shRNA, short-hairpin RNA; TIRF, total internal reflection fluorescence.

periphery via this tripartite protein complex, melanosomes are clustered at the perinuclear region through microtubule-dependent translocation and therefore cannot be transferred to neighboring keratinocytes. A similar but distinct complex consisting of Rab27a, exophilin8/MyRIP/Slac2-c, and myosin VIIa, is proposed to function on retinal melanosomes in the retinal pigment epithelium (El-Amraoui *et al.*, 2002). Exophilin8 shares amino acid homology with melanophilin and binds Rab27a through the N-terminal region and myosin Va/VIIa and/or actin through the C-terminal region, although the endogenous association of exophilin8 with myosin Va or VIIa has not been demonstrated (El-Amraoui *et al.*, 2002; Fukuda and Kuroda, 2002; Ramalho *et al.*, 2009). These findings suggest that, as with melanophilin on skin melanosomes, exophilin8 acts as a linker in the F-actin–dependent capture of retinal melanosomes. Exophilin8 is also expressed on secretory granules in endocrine cells such as chromaffin and pancreatic β cells, and the altered expression of exophilin8 has been reported to affect granule exocytosis in their corresponding cell lines, PC12 and INS-1, although the effects vary across studies (Desnos *et al.*, 2003; Waselle *et al.*, 2003). Overall, the precise function of exophilin8 in granule exocytosis has yet to be determined.

In the present study, we examined the roles of exophilin8 on insulin granule location and exocytosis. We found that exophilin8 concentrates insulin granules at the corners of pancreatic β cells and their cell line, MIN6, where both microfilaments and microtubule plus-end bundles are enriched. Exophilin8-positive granules locate at a region deeper than that where another Rab27a effector, granuphilin, accumulates granules directly docked to the plasma membrane (Gomi *et al.*, 2005). Furthermore, exophilin8 and exophilin8-positive granules show markedly low protein turnovers and organelle movements, even compared with granuphilin and granuphilin-positive docked granules. However, granules are released from exophilin8-induced immobility and readily fuse to the plasma membrane upon secretory stimulation. Moreover, attenuation of exophilin8 expression inhibits the delivery and fusion of granules to the plasma membrane. These findings indicate that exophilin8 captures and stores insulin granules for subsequent release into the cortical actin network near the microtubule plus-end bundles.

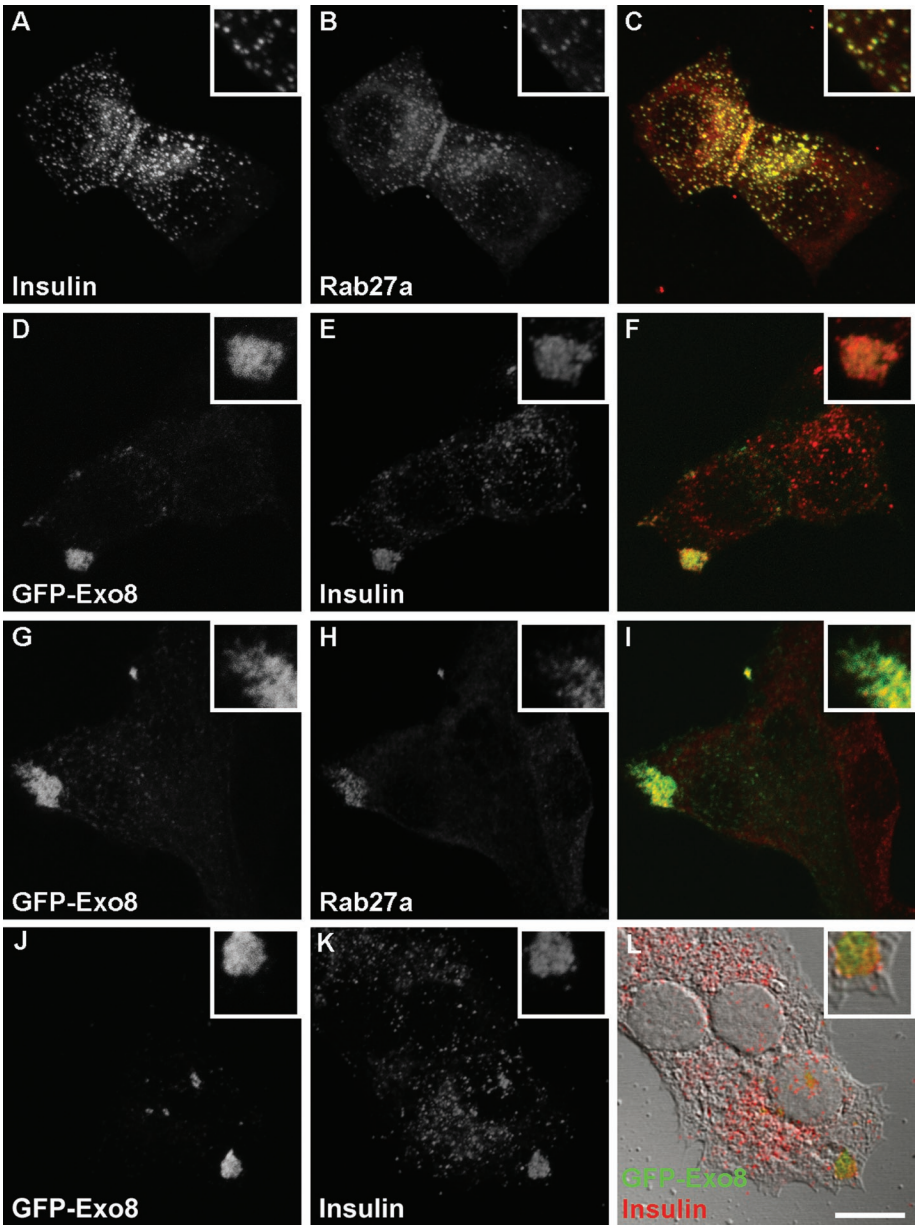

FIGURE 1: Localization of exophilin8 on insulin granules in MIN6 cells. MIN6 cells without (A–C) or with infection of adenovirus encoding EGFP-fused exophilin8 (GFP-Exo8; D–L) were double-imaged for insulin (A, E, and K), Rab27a (B and H), and GFP-Exo8 (D, G, and J) with a confocal laser scanning microscope. Panels C, F, and I show the merged images. The images in (J) and (K) are merged into the differential interference contrast microscopic image in (L). The detail is shown at a higher magnification (insets). Bar, 10 μm.

RESULTS

Exophilin8 accumulates insulin granules at the cell corner

Exophilin8 is expressed in pancreatic β cells and colocalized with insulin granules in their cell line INS-I (Waselle *et al.*, 2003). We first examined the effect of exophilin8 protein expression on insulin granule distribution. In the mouse pancreatic β-cell line MIN6, insulin granules were widely diffused throughout the cytosol and colocalized with Rab27a (Figure 1, A–C), as shown previously (Yi *et al.*, 2002). When MIN6 cells were infected with recombinant adenovirus encoding enhanced green fluorescent protein (EGFP)-tagged exophilin8 (GFP-Exo8), GFP-Exo8 was concentrated at the cell corners, where insulin and Rab27a were also redistributed (Figure 1, D–I). This effect was also observed in primary pancreatic β cells isolated from mice (Supplemental Figure 1). These findings indicate that apparently nonpolarized β cells possess machinery that orients granules to the cell corners in response to exophilin8 expression. Exophilin8-positive insulin granule clusters were not found to be directly attached to the cell membrane (Figure 1, J–L). Thus the granule

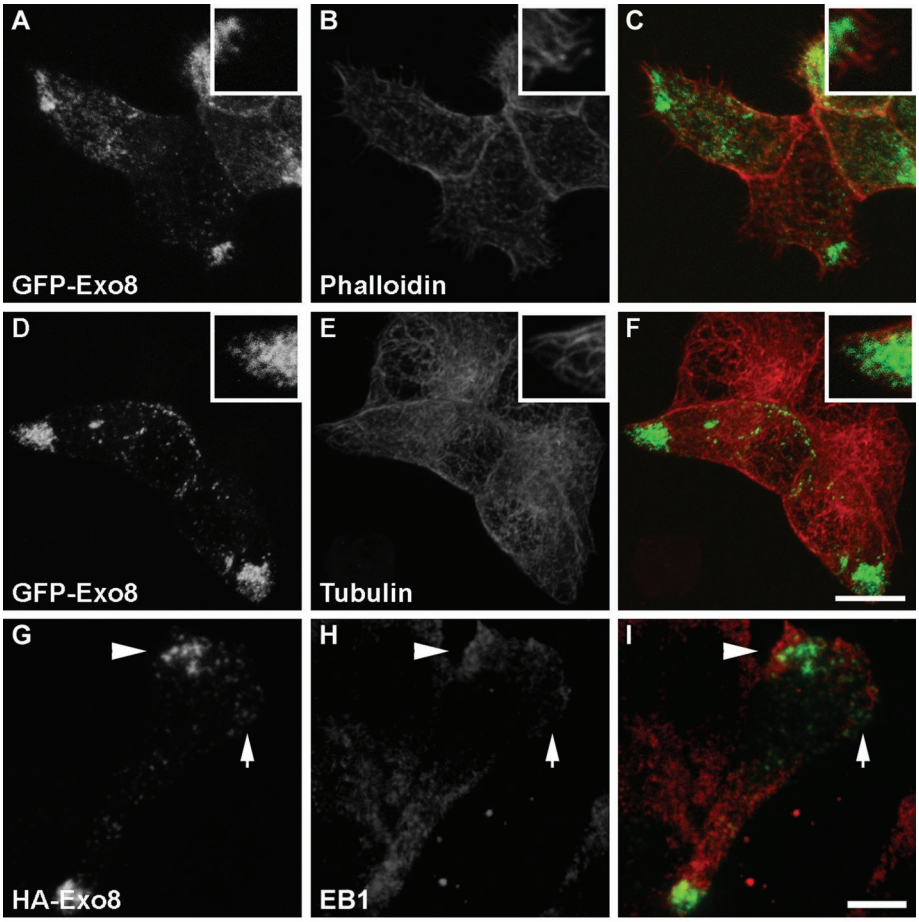

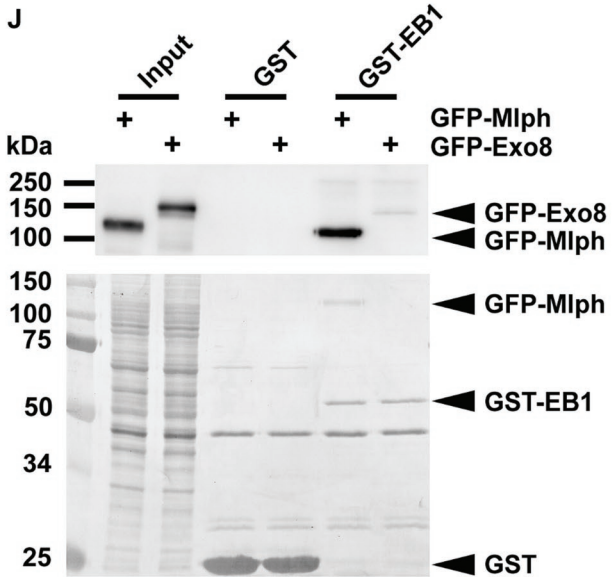

FIGURE 2: Relationship of exophilin8 with cytoskeletal components. (A–I) MIN6 cells were infected with adenovirus encoding either EGFP-fused exophilin8 (GFP-Exo8; A–F) or HA-tagged exophilin8 (HA-Exo8; G–I). They were double-imaged by confocal microscopy for GFP-Exo8 (A and D) and rhodamine-phalloidin (B) or α-tubulin (E), or by dual-color TIRF microscopy for HA-Exo8 (G) and EB1 (H). Note that the signal strengths of HA-Exo8 are correlated with those of EB1 (compare the cell corner indicated by an arrowhead with that by an arrow in G–I). Panels C, F, and I show the merged images. The detail was shown at a higher magnification (insets). Bars, 10 μm. (J) HEK293 cells were transfected with a plasmid encoding EGFP-fused melanophilin (GFP-Mlph) or GFP-Exo8. The cell lysates were incubated with GST alone or GST-fused EB1 (GST-EB1). The interacting proteins as well as aliquots of the original lysates (input) were analyzed by immunoblotting with anti–GFP antibody (top) followed by Coomassie brilliant blue R-250 staining (bottom).

location induced by exophilin8 was quite different from that displayed with another Rab27a effector, granuphilin, which redistributes insulin granules along the plasma membrane (Torii *et al.*, 2004).

Exophilin8-induced gross granule redistribution at cell corners may involve cytoskeletal components. In fact, exophilin8 has been shown to possess binding activity toward actin both directly and through interaction with the motor proteins myosin Va and VIIa (El-Amraoui *et al.*, 2002; Fukuda and Kuroda, 2002). Although there were no obvious differences in cellular F-actin and microtubule structures between MIN6 cells with and without exophilin8 expression, both phalloidin-positive needle-like structures and α-tubulin–positive fiber ends accumulated at the GFP-Exo8–positive corners (Figure 2, A–F). Strikingly, the microtubule plus-end binding protein, EB1, also localized with exophilin8 at the corners, even within an evanescent field observed by a total internal reflection fluorescence (TIRF) microscope (Figure 2, G–I). The signal strengths of EB1 at the cell corners were correlated with those of exophilin8. These findings indicate that, at least under the present culture condition, exophilin8 preferentially accumulates insulin granules at the leading edge-like structure, which has been characterized in migrating fibroblasts by membrane ruffling, filopodia formation, and capture of microtubule plus-ends (Noritake *et al.*, 2005). It has been reported that another Rab27a effector, melanophilin, directly interacts with EB1 through the C-terminal region and behaves as a microtubule plus-end tracking protein in living fibroblasts and melanocytes (Wu *et al.*, 2005). Among the Rab27 effector family proteins (Izumi, 2007), exophilin8 and melanophilin share a C-terminal region showing binding activities toward actin and myosin Va (Fukuda and Kuroda, 2002). Thus we explored the possibility that exophilin8 could also bind EB1. However, recombinant EB1 protein interacted scarcely with exophilin8, although it did so efficiently with melanophilin (Figure 2J).

Exophilin8 binds Rab27a through the N-terminal region and to myosin Va/VIIa and actin through the C-terminal region (El-Amraoui *et al.*, 2002; Fukuda and Kuroda, 2002). To evaluate the significance of these interactions in the granule-clustering activity, we prepared two exophilin8 point mutants, R35W and A748P, based on the sequence similarity between exophilin8 and melanophilin. Exophilin8 R35W corresponds to melanophilin R35W, which specifically disrupts interaction with Rab27a (Ménasché

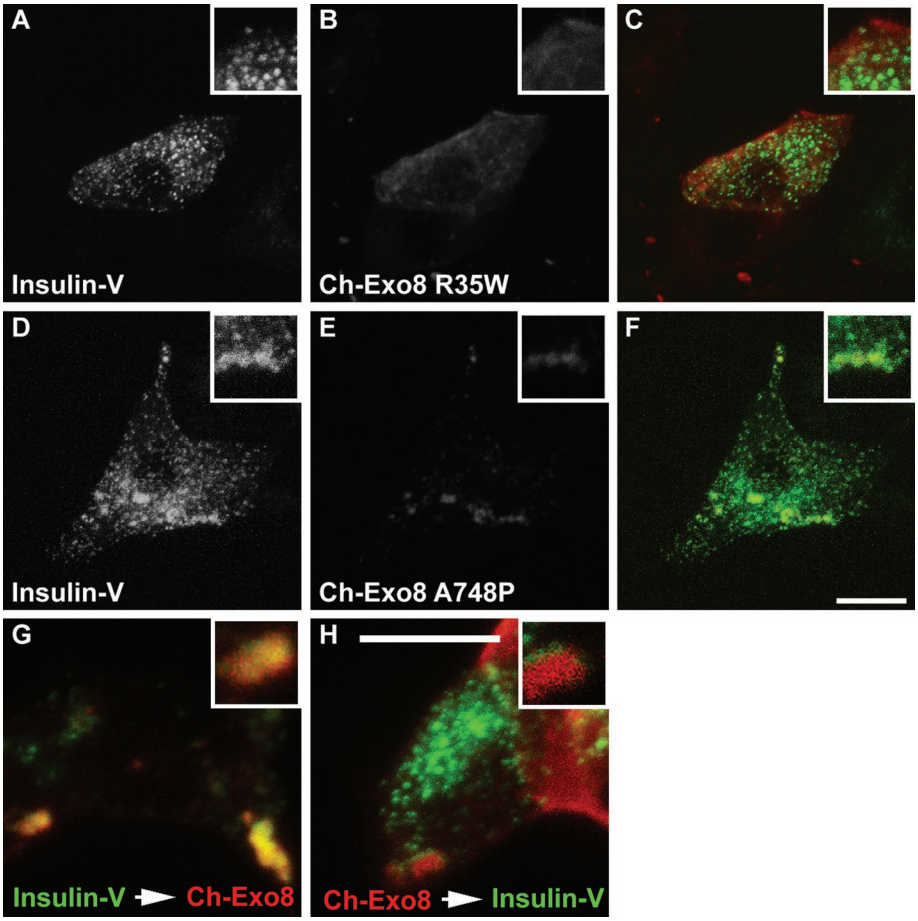

FIGURE 3: Effects of wild-type and mutant exophilin8 expression on insulin granule distribution. (A–F) MIN6 cells were coinfected by adenoviruses encoding preproinsulin-Venus (Insulin-V) and mCherry-fused exophilin8 (Ch-Exo8) R35W (A–C) or A748P (D–F) at moi 5, respectively. Two days after the infection, the cells were double-imaged for Insulin-V (A and D) and Ch-Exo8 (B and E) by confocal microscopy. Panels C and F show the merged images. (G and H) MIN6 cells were first infected with adenovirus encoding Insulin-V (G) or wild-type Ch-Exo8 (H). A day after the infection, the cells were then infected with adenovirus encoding Ch-Exo8 (G) and Insulin-V (H), respectively. The cells infected in tandem were double-imaged for Insulin-V and Ch-Exo8 by confocal microscopy. The detail is shown at a higher magnification (insets). Bars, 10 μm.

et al., 2003), whereas exophilin8 A748P corresponds to melanophilin A467P that fails to interact with the cargo-binding tail of myosin Va (Hume *et al.*, 2006). In fact, exophilin8 R35W lost the binding activity toward Rab27a (Supplemental Figure 2), whereas exophilin8 A748P has recently been shown to exhibit a severely reduced binding activity to the myosin Va tail (Ramalho *et al.*, 2009). When MIN6 cells were coinfected with recombinant adenoviruses encoding mCherry-tagged, wild-type exophilin8 (Ch-Exo8), and preproinsulin-Venus (Insulin-V), Ch-Exo8, like GFP-Exo8, accumulated at the cell corners and concentrated the insulin granules there (not shown; see Figure 3G for the cells infected in tandem). By contrast, Ch-Exo8 R35W exhibited a diffuse cytosolic distribution and did not change Insulin-V localization (Figure 3, A–C). Although Ch-Exo8 A748P showed a punctate pattern and partial colocalization with Insulin-V, the double-positive structures were larger than insulin granules and never clustered at the corners (Figure 3, D–F). These findings indicate that interactions with both Rab27a and myosin Va are essential for exophilin8-induced granule clustering at the cell corners. We then infected MIN6 cells in series at an interval of 24 h by adenovirus encoding Insulin-V followed by that encoding wild-type Ch-Exo8. Ch-Exo8 was colocalized with Insulin-V at the cell corners (Figure 3G), as was found in the cells infected simultaneously. However, the MIN6 cells that were infected in a reciprocal order exhibited little overlap between the signals (Figure 3H), suggesting that the initially expressed Ch-Exo8 already clusters unlabeled insulin granules and cannot accumulate newly labeled granules. These observations suggest that exophilin8 forms a stable granule cluster at the cell corners.

Exophilin8 stably immobilizes insulin granules near the plasma membrane

Due to the suggested stability of exophilin8-positive structures, we next performed fluorescence recovery after photobleaching (FRAP) analysis for the GFP-Exo8 concentrated at the corners of MIN6 cells (Figure 4A). As shown by a representative kymograph over 200 s (Figure 4B), the fluorescence recovery was minimal (Figure 4C; 0.1 ± 1.2% at 3 min, n = 5), suggesting that GFP-Exo8 is steadily located on the cytosolic surface membrane of insulin granules. In contrast, the levels of fluorescence recovery for GFP-fused Rab27a (GFP-Rab27a) and its effector, granuphilin (GFP-Grph), were much higher (9.4 ± 1.1%, n = 7; and 19.0 ± 2.5%, n = 9, respectively). These values are roughly equivalent to those previously examined for EGFP-fused Rab27a and granuphilin in PC12 cells (Handley *et al.*, 2007; Handley and Burgoyne, 2008). Thus exophilin8 exhibits a markedly low protein turnover rate on insulin granules.

We next examined insulin granule motion near the plasma membrane by TIRF microscopy in MIN6 cells expressing Insulin-V, GFP-Exo8, or GFP-Grph (Figure 5A). The mobility of the fluorescent punctate structures was analyzed in 10-s sequences of 120 frames. As shown in Figure 5B, the median value of a two-dimensional diffusion coefficient D*x,y* for Insulin-V was calculated at 13.5×10^{-5} μm^2/s (n = 52 patches from 9 cells). The diffusion coefficient for GFP-Grph was much lower than that of Insulin-V and was estimated to be 4.2×10^{-5} μm^2/s (n = 110 patches from 16 cells), which may reflect the immobile nature of granuphilin-mediated docked granules. Notably, the median D*x,y* for GFP-Exo8 was even lower, at 3.3×10^{-5} μm^2/s (n = 58 patches from 13 cells). These observations indicate that the motion of exophilin8-positive granules was severely restricted. We noticed under TIRF microscopy that the signal strengths of GFP-Exo8–positive punctate structures are flat and faint, compared with the significantly varied strengths of Insulin-V–positive structures (Figure 5A). We speculated that GFP-Exo8–positive granules are stacked at a specific site located relatively far from the plasma membrane as compared with granuphilin-positive granules. To investigate this possibility, we estimated the granule position from the glass–water interface. Considering the exponential decay characteristic of the evanescent field, the intensities of individual spots were transformed into the *z* distance. The calculated distances were classified into bins of 10-nm intervals (Figure 5C). There were two peaks

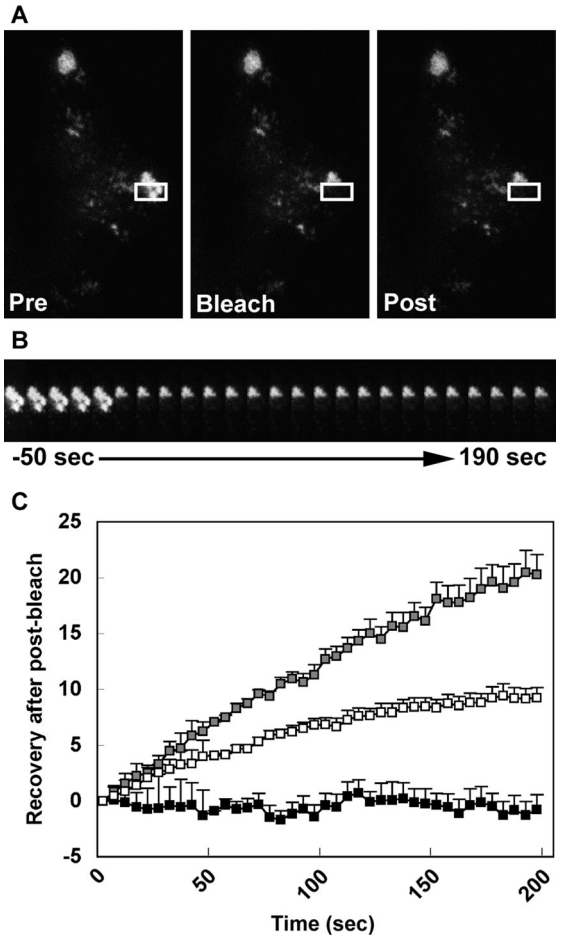

FIGURE 4: Dynamics of Rab27a and its effectors on insulin granules in MIN6 cells. (A) MIN6 cells were infected with adenovirus encoding EGFP-fused exophilin8 (GFP-Exo8). The region of interest (white squares) was bleached at time 0 with a high-intensity laser. (B) The kymograph showed the fluorescence recovery at 10-s intervals from −50 s to 190 s. (C) The fluorescence recovery of GFP-Exo8 (black squares) as well as that analyzed similarly for EGFP-fused granuphilin (GFP-Grph, gray squares) and Rab27a (GFP-Rab27a, white squares) were normalized and are shown as means ± SEM.

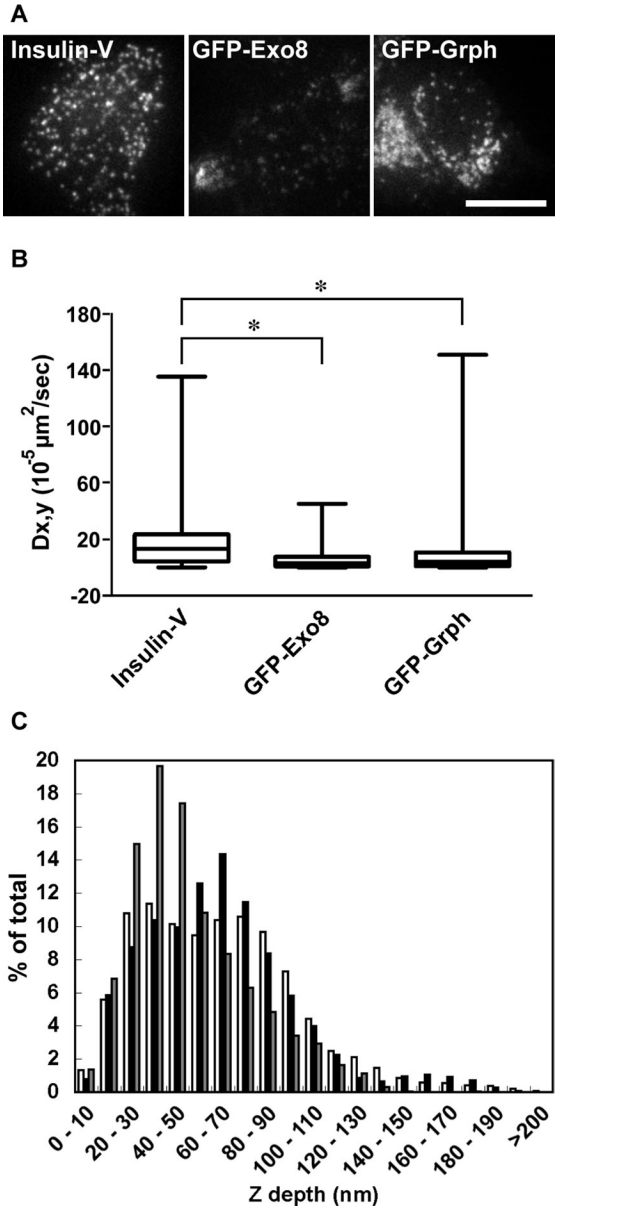

FIGURE 5: Motion and depth of exophilin8-positive insulin granules near the plasma membrane. (A) MIN6 cells were infected with adenovirus encoding preproinsulin-Venus (Insulin-V), EGFP-exophilin8 (GFP-Exo8), or EGFP-granuphilin (GFP-Grph). The cells were subjected to live cell imaging by a TIRF microscope with a penetration depth of 100 nm. Representative images are shown. Bar, 10 µm. (B) The TIRF images were taken every 82.9 ms over 200 time points. The GFP-positive structures were tracked, and the 2D diffusion coefficient D*x,y* was calculated. Data are shown as box-plots: a box and a bar within the box indicate the 25–75% range and a median value, respectively, whereas outer bars represent minimum and maximum values. The statistical significance of differences was assessed by a Kruskal–Wallis test followed by Dunn's post test (*, $P < 0.05$). (C) The maximal fluorescence intensity corrected for background intensity was obtained from a TIRF image. Then the intensities of individual GFP-positive patches were converted to the *z* distance considering the exponential decay characteristic of the evanescent field. The relative *z* positions from the evanescent field origin of Insulin-V (white bars), GFP-Exo8 (black bars), and GFP-Grph (gray bars) were categorized into bins of 10 nm in width and expressed as the fraction of the total patches analyzed.

in a profile of Insulin-V: one from 30 to 40 nm and the other from 70 to 80 nm; GFP-Exo8, however, showed a monotonous peak from 60 to 70 nm, roughly overlapping with the deeper peak of Insulin-V. By contrast, the *z* position profile of GFP-Grph exhibited a single peak from 30 to 40 nm, corresponding to the shallower peak of Insulin-V, which is consistent with the function of granuphilin in the docking of insulin granules to the plasma membrane (Torii *et al.*, 2004; Gomi *et al.*, 2005). These findings suggest that exophilin8-positive insulin granules cannot approach as close to the plasma membrane as granuphilin-positive docked granules.

Exophilin8 promotes insulin release

We then examined the effect of exophilin8 expression on insulin granule release. As shown in Figure 6A, we first confirmed that the amplitude and time course of the depolarization-induced rise of the intracellular Ca^{2+} concentration were similar between MIN6 cells with and without expression of hemagglutinin (HA)-tagged exophilin8 (HA-Exo8). We then monitored the fusion events of insulin granules labeled by Insulin-V using TIRF microscopy. In the 5 min after depolarization stimulation, we observed at total of 30.0 ± 4.1

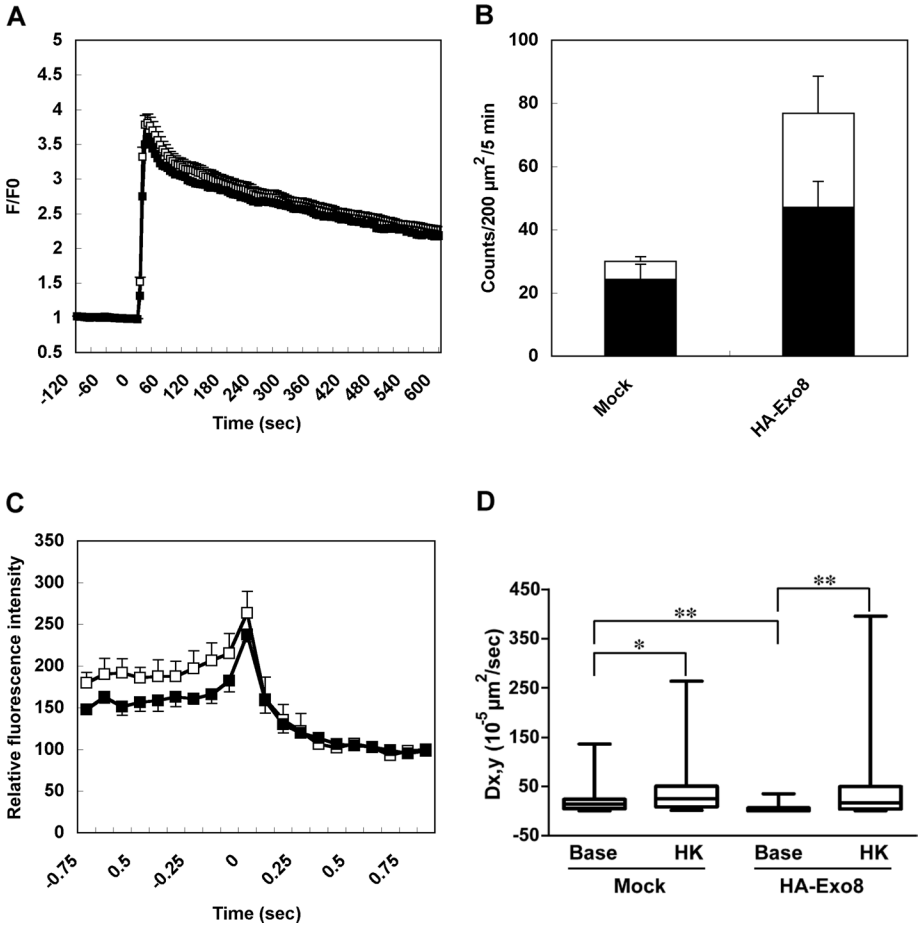

FIGURE 6: Insulin release from MIN6 cells expressing exophilin8. (A) MIN6 cells without (open squares, n = 70 cells from 5 fields) or with infection of adenovirus encoding HA-tagged exophilin8 (HA-Exo8; closed squares, n = 58 from 4 fields) were loaded with a Ca^{2+} indicator, Fluo-4, and stimulated by 60 mM KCl. The Fluo-4 fluorescence was defined as the change from initial (time 0) fluorescence (ΔF/F0). (B) MIN6 cells were infected with adenovirus encoding preproinsulin-Venus (Insulin-V) without or with infection of adenovirus encoding HA-Exo8. After 2 d, the infected cells were preincubated with KRB at 37°C for 30 min and the images were acquired by TIRF microscopy every 82.9 ms over 10 min. Ninety seconds after image acquisition, the cells were stimulated by 60 mM KCl. The black columns correspond to the number of fusion events from "resident" granules within an evanescent field prior to the stimulation, whereas the white columns correspond to those from "passenger" granules that are newly recruited from the outside of an evanescent field and immediately fused to the plasma membrane. Data are expressed as means ± SEM (n = 9 for control cells and n = 4 for the cells expressing HA-Exo8). The statistical significance of differences was assessed by a Mann–Whitney U test (*, $P < 0.05$). (C) The fluorescence changes were measured in the center of Insulin-V–positive granules in MIN6 cells without (open squares) or with infection of adenovirus encoding HA-Exo8 (closed squares). The average fluorescence intensity after fusion was set equal to 100% (n = 7 each). (D) Insulin-V–positive granules were tracked during 30 s in a basal state starting at 1 min before stimulation (base) and during 30 s in a stimulated state starting at 30 s after 60 mM KCl stimulation (HK). The 2D diffusion coefficient D*x,y* was derived from the slope of a curve in the MSD vs. time plot. Data are shown as box-plots: a box and a bar within the box indicate the 25–75% range and a median value, respectively, whereas outer bars represent minimum and maximum values. The statistical significance of differences was assessed by a Mann–Whitney U test (*, $P < 0.05$; **, $P < 0.01$).

insulin-release events per 200 μm² from mock-infected MIN6 cells (n = 9). We previously categorized fused granules into the following three types based on their visibility in the prefusion step in mouse pancreatic β cells: those visible before stimulation, "residents"; those that become visible during the stimulation, "visitors"; and those that fuse without stably docking, "passengers" (Kasai *et al.*, 2008). Because it was rare to observe the "visitor" type of fusion during depolarization-induced insulin secretion in MIN6 cells (Supplemental Video 1), we categorized the fused granules into two types, "residents" and "passengers." As reported previously in mouse pancreatic β cells (Kasai *et al.*, 2008), depolarization-induced insulin release mainly occurred from "resident" granules in MIN6 cells (Figure 6B and Supplemental Video 1). The same treatment induced 76.9 ± 17.9 events from MIN6 cells expressing HA-Exo8 (n = 4). Therefore exophilin8 expression enhanced evoked exocytosis of insulin granules. Interestingly, the "passenger" type of insulin release was much more frequent in those cells compared with control cells (29.8 ± 11.8 vs. 5.7 ± 1.4 events; Figure 6B and Supplemental Video 2). Moreover, fluorescence intensity measurement during the "resident" type of fusion in the cells expressing HA-Exo8 revealed weaker initial fluorescence intensity than that in control cells, although the overall time course of fluorescence changes was not affected (Figure 6C). These findings suggest that exophilin8-positive insulin granules fuse from a relatively deeper position, which is consistent with the *z* position profile of GFP-Exo8 in a steady state (Figure 5C). Because exophilin8-positive structures were markedly immobile in an unstimulated state (Figure 5B), we directly compared the mobility of Insulin-V–labeled granules between basal and stimulated states by TIRF microscopy (Figure 6D). As shown already in Figure 5B, the median value of a diffusion coefficient D*x,y* in mock infected cells was 13.5×10^{-5} μm²/s in a basal state (n = 52 granules from 9 cells). By contrast, the value in cells expressing HA-Exo8 was 3.9×10^{-5} μm²/s (n = 55 granules from 12 cells). Thus exophilin8 expression significantly reduced the diffusion coefficient of Insulin-V, consistent with that of GFP-Exo8 itself (Figure 5B). This finding is in agreement with the previous finding that exophilin8 expression reduces the mobility of secretory granules in PC12 cells (Desnos *et al.*, 2003). Importantly, stimulation by 60 mM KC1 increased the median coefficient in mock infected cells to 24.5×10^{-5} μm²/s (n = 36 granules from 9 cells). The corresponding value in cells expressing HA-Exo8 similarly stimulated was 12.4×10^{-5} μm²/s (n = 52 granules from 12 cells), which was not significantly different from that in the control cells. Therefore insulin granule motion was enhanced under the stimulated state, and the evoked granule motion and exocytosis were not inhibited by exophilin8 expression.

Functional requirement of exophilin8 for insulin granule exocytosis

The dominant effects of exogenously expressed exophilin8 on granule localization and exocytosis prompted us to investigate its

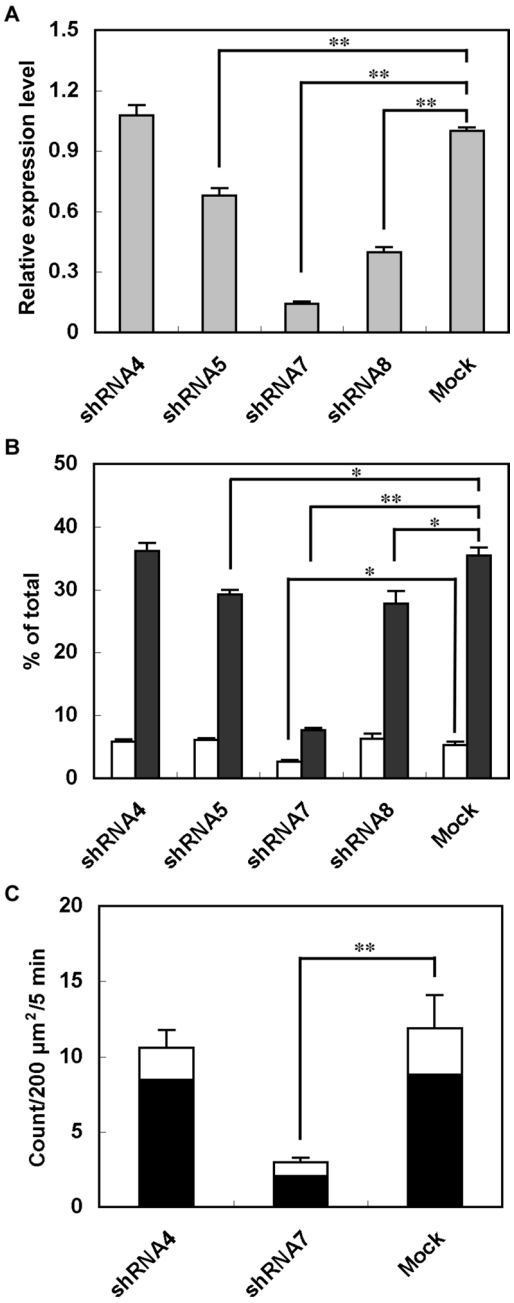

FIGURE 7: Effects of exophilin8 knockdown on insulin release from MIN6 cells. (A) Exophilin8 mRNA expression levels were determined by real-time quantitative PCR in MIN6 cells without or with infection of adenoviruses encoding exophilin8-specific shRNAs. The mean expression level in mock-treated cells was set at one. (B) MIN6 cells expressing exophilin8-specific shRNAs were incubated for 10 min with KRB (white bars) or KRB containing 60 mM KCl (black bars). The amount of insulin in the medium was normalized to total insulin content. (C) MIN6 cells expressing NPY-KO1 (n = 8) and those coexpressing noneffective shRNA4 (n = 7) or strongly effective shRNA7 (n = 6) were observed with a TIRF microscope. The NPY-KO1 images were acquired every 50 ms over 10 min in cells expressing shRNAs identified by EGFP fluorescence. Ninety seconds after image acquisition, the cells were stimulated by 60 mM KCl. The black columns correspond to the number of fusion events from "resident" granules, whereas the white columns correspond to those from "passenger" granules. Data are expressed as means ± SEM. The statistical significance of differences was assessed by a Mann–Whitney U test (*, $P < 0.05$; **, $P < 0.01$ vs. Mock).

physiological involvement in the secretory process. As there is no available animal model to examine exophilin8 loss-of-function, we infected MIN6 cells with adenoviruses encoding EGFP and exophilin8-specific short-hairpin RNAs (shRNAs; Lopes *et al.*, 2007). Out of four shRNAs, three (shRNA5, -7, and -8) led to significant decreases in the level of exophilin8 mRNA, whereas one (shRNA4) had no effect (Figure 7A). The ability of each shRNA to reduce the level of endogenous exophilin8 mRNA in MIN6 cells is consistent with the previously reported decrease of exogenous exophilin8 protein in HEK-293FT cells (Lopes *et al.*, 2007). Batch insulin secretion assays revealed that attenuation of exophilin8 expression decreased depolarization-induced insulin release in a manner correlated with the efficacy of each silencer (Figure 7B). The strongest silencer, shRNA7, also reduced basal secretion. We then investigated fusion events of individual insulin granules by TIRF microscopy in MIN6 cells doubly infected with adenovirus encoding the exophilin8 shRNA and that encoding neuropeptide Y (NPY) fused with Kusabira-Orange 1 (KO1). Fusion events of NPY-KO1–labeled insulin granules were directly monitored in shRNA-expressing, EGFP fluorescence–positive cells (Figure 7C). In the 5 min after depolarization stimulation, we observed a total of 11.9 ± 2.2 insulin-release events per 200 μm^2 from mock-infected MIN6 cells (n = 8) and 10.6 ± 1.2 events from MIN6 cells expressing noneffective shRNA4 (n = 7). By contrast, a profound decrease was found in cells expressing the strongly effective silencer shRNA7 (3.0 ± 0.3 events, n = 6). Thus exophilin8 depletion severely reduced evoked exocytosis of insulin granules.

We then examined the effect of exophilin8 knockdown on granule localization. The total number of granules visualized by TIRF microscopy was significantly reduced in cells expressing effective silencers but not in those expressing noneffective ones (Figure 8A). The decrease in the number of granules underneath the plasma membrane was again correlated with the efficacy of each silencer (Figures 7A and 8B). Alterations in granule distribution were also detected by confocal microscopy (Supplemental Figure 3). Although insulin granules frequently concentrated along the cell–cell junctions in MIN6 cells, it was rare to observe such granule accumulation in exophilin8-depleted cells (Supplemental Figure 3, arrowheads). These findings suggest that insulin granules fail to arrive close to the plasma membrane in the absence of exophilin8. Taken together, exophilin8 is likely to play a pivotal role in insulin secretion by transiently trapping granules near the plasma membrane to promote the granule supply to fusion sites during secretagogue stimulation.

DISCUSSION

We have shown that exogenous expression of exophilin8 concentrates insulin granules at the cell corners of pancreatic β cells and their cell line, MIN6. These findings indicate that, despite the apparent lack of distinct cell polarity, β cells have the intrinsic machinery to polarize insulin granules to a highly restricted position. Although exophilin8-induced granule redistribution has not been reported, exophilin8 itself localizes in specific sites in other cells: it accumulates at the tips of neurites in differentiated PC12 cells (El-Amraoui *et al.*, 2002; Desnos *et al.*, 2003), and, in the β cell line INS-1, it is most dense at the dendritic-like protrusions, where insulin granules already accumulate (Waselle *et al.*, 2003). These findings suggest that exophilin8 tends to localize at a restricted peripheral area in endocrine cells.

The granule redistribution pattern induced by exophilin8 is in marked contrast to that of another Rab27a effector, granuphilin, which accumulates granules along the plasma membrane (Torii *et al.*, 2004). Confocal microscopy has revealed that the exophilin8-positive site is not directly attached to the plasma membrane.

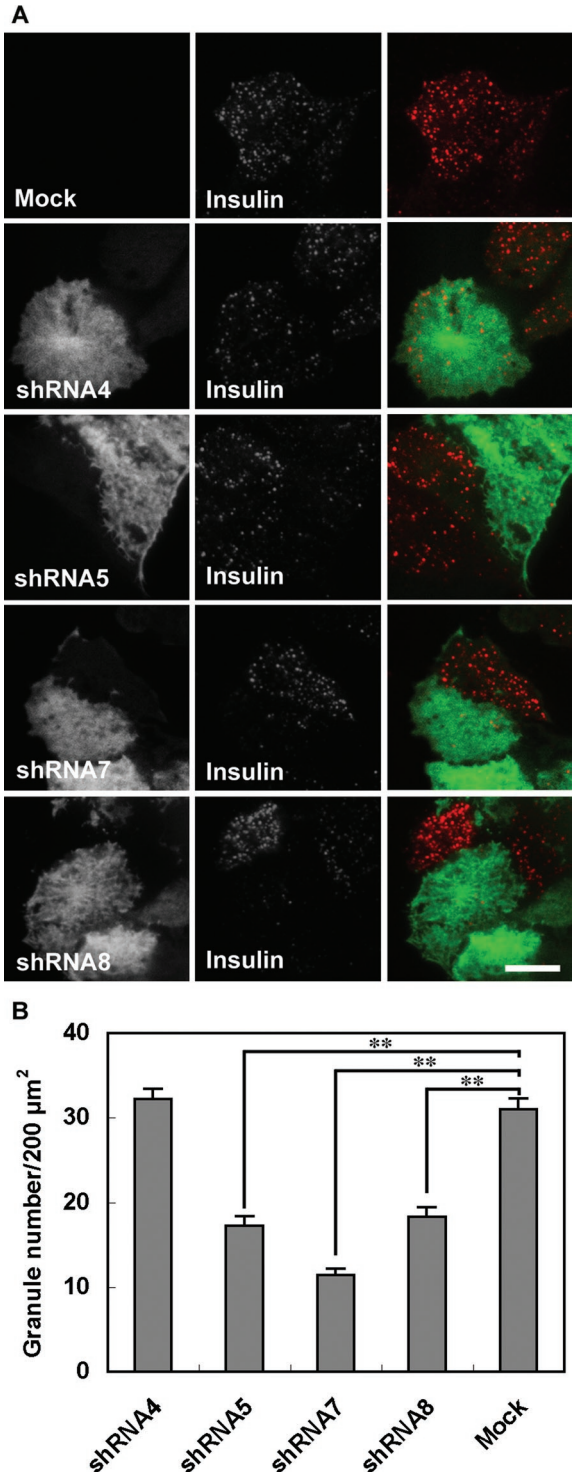

FIGURE 8: Effects of exophilin8 knockdown on insulin granule density near the plasma membrane. MIN6 cells were infected with recombinant adenovirus allowing expression of EGFP and the indicated exophilin8 shRNA. After 2 d, the infected cells as well as uninfected MIN6 cells were fixed and immunostained with anti–insulin antibody. (A) The cells were double-imaged for EGFP (left) and insulin (middle) with a TIRF microscope. Merged images were also shown (right). Bar, 10 μm. (B) The number of insulin granules identified in the evanescent field (calibrated at ~100 nm from the coverslip) per adherent membrane area unit (200 μm^2) are represented as means ± SEM (n = 41–54). The statistical significance of differences was assessed by a Mann–Whitney U test (**, $P < 0.01$ vs. Mock).

Furthermore, TIRF microscopy differentially discriminates the *z* positions of the two Rab27a effectors: exophilin8 locates in a deeper interior area, whereas granuphilin locates just beneath the plasma membrane consistent with its role in granule docking to the plasma membrane (Gomi *et al.*, 2005). It is well established that secretory cells have a continuous ring of actin filaments underneath the plasma membrane and that many granules are retained within the cortical actin network (Trifaró and Vitale, 1993). Consistent with the ability to bind myosin Va/VIIa and/or actin (El-Amraoui *et al.*, 2002; Fukuda and Kuroda, 2002), the exophilin8-positive cell corners harbored microfilaments. Furthermore, the exophilin8 A748P mutant that is deficient in myosin Va binding activity (Ramalho *et al.*, 2009) failed to accumulate granules at the corners. These findings suggest that cortical actin filaments are involved in the localization of the exophilin8-positive granules. However, other factors must also play a role because exophilin8 is not distributed along the cell circumference in the pattern of cortical actin but instead specifically concentrates at the corners. We found that exophilin8 locates with a brush tip–like structure of microtubules and the microtubule plus-end protein, EB1, within a narrow evanescent field. We explored a possible interaction of exophilin8 with EB1 because another Rab27a effector, melanophilin, is known to interact with EB1 (Wu *et al.*, 2005). However, exophilin8 scarecely bound EB1. This finding is consistent with the fact that a Ser-X-Ile-Pro motif important for the interaction with EB1 (Slep *et al.*, 2005; Honnappa *et al.*, 2009) is conserved in melanophilin but not in exophilin8. Although the molecular determinants of the exophilin8 location have yet to be determined, our findings suggest that exophilin8 transfers newly formed granules from microtubules to microfilaments near the microtubule plus-ends. This transfer appears to be a crucial step for the delivery and fusion of insulin granules to the plasma membrane because exophilin8-depleted MIN6 cells exhibit marked decreases in the number of granules close to the plasma membrane and in that of fusion events.

FRAP analysis and TIRF microscopy have shown that exophilin8 and exophilin8-associated granules are extremely stable and immobile. These findings are consistent with the previous TIRF-microscopic finding that exophilin8 restricts the motion of secretory granules in PC12 cells (Desnos *et al.*, 2003). It has been proposed that myosin Va, a possible partner of exophilin8, might mediate the docking of secretory granules to the plasma membrane because of its contribution to the long-lasting immobilization of granules beneath the plasma membrane (Desnos *et al.*, 2007). We, however, prefer the interpretation that exophilin8 and possibly myosin Va function at a more interior area within the cortical actin network, because of the differential locations between exophilin8 and granuphilin, the latter of which has been demonstrated by electron microscopy to be essential for the direct attachment of granules to the plasma membrane (Gomi *et al.*, 2005). Consistent with this idea, we showed by TIRF microscopy that exophilin8 promotes exocytosis from granules located at deeper positions. This observation also supports our previous proposal that stable docking is not a prerequisite for fusion of insulin granules (Izumi *et al.*, 2007; Kasai *et al.*, 2008).

The cortical actin network is generally thought to act as a physical barrier for granule exocytosis (Trifaró and Vitale, 1993). If exophilin8 traps granules into the network, it may inhibit granule exocytosis. In the present study, however, despite the marked immobility of insulin granules in the basal state, exophilin8 did not inhibit evoked exocytosis but did increase the depolarization-induced secretory response, especially from newly recruited granules. Moreover, attenuation of exophilin8 expression by RNA interference impaired

the depolarization-induced secretory response in MIN6 cells, which is consistent with the finding previously reported using a similar RNA interference strategy in another β-cell line, INS-1 (Waselle *et al.*, 2003). On the contrary, overexpression of exophilin8 in PC12 cells has been shown to moderately reduce the depolarization-induced secretory response (Desnos *et al.*, 2003). The variability in the findings regarding the effect of exophilin8 on the secretory response may reflect differences in the cell lines and in the expression level ratios of exogenous versus endogenous exophilin8. However, we found that depolarization stimulation increases the mobility of secretory granules and, more notably, that exophilin8-induced granule immobility is canceled upon the stimulation. A secretagogue-induced Ca^{2+} influx regulates many actin-binding proteins and causes dissolution of the cortical F-actin (Trifaró *et al.*, 2008), which could result in granule detachment and give the granules free access to the exocytic site on the plasma membrane. Secretagogue-induced depolymerization of cortical F-actin has also been observed in pancreatic β and MIN6 cells (Thurmond *et al.*, 2003). Therefore exophilin8-mediated, transient granule immobilization likely represents a physiological step to store granules in the cortical actin network for subsequent release.

MATERIALS AND METHODS

Construction of plasmids and recombinant adenoviruses

The cDNA encoding a full open reading frame of murine exophilin8 was amplified from cDNAs of MIN6 cells by PCR. It was then inserted into the *Eco*RI site of pEGFP-C1 and pmCherry-C1 vectors using the In-Fusion PCR Cloning System (Clontech, Mountain View, CA) and the following primers (flanking sequence underlined): 5′-CTCAAGCTTCGAATTTCATGGGGAGGAAGCTGGAC-3′ and 5′- GTCGACTGCAGAATTTTAGTACATCACAGCTGACTCC-3′. The full-length cDNAs of murine melanophilin and EB1 were similarly amplified using the following pairs of primers: 5′-CCGGAATTCATGGGGAAAAGGTTGGACCTTTC-3′ and 5′-CCGCTCGAGTTAGGGCTGCTGGGCCATCA-3′ (melanophilin), and 5′-CTCAAGCTTCGAATTCGATGGCAGTGAATGTGTACTC-3′ and 5′-GTCGACTGCAGAATTGCTTAATACTCTTCTTGTTCCTC-3′ (EB1). The melanophilin cDNA was subcloned into the *Eco*RI and *Xho*I sites of pEGFP-C2 vector. The EB1 cDNA directly inserted into the *Eco*RI-digested pEGFP-C1 vector was cut out as a *Bgl*II-*Sma*I fragment and then subcloned into the *Bam*HI and *Sma*I sites of pGEX4T-1 (GE Healthcare, Little Chalfont, UK). Site-directed mutagenesis of exophilin8 cDNA was carried out using the following pairs of primers: 5′-GAGGAGGACTGGCTAAGTGAG-3′ and 5′-CTCACTTAGCCAGTCCTCCTC-3′ (R35W), and 5′-GTGCACCACCCCGAACTCCA-3′ and 5′-TGGAGTTCGGGGTGGTGCAC-3′ (A748P). A full-length human preproinsulin cDNA in the pEGFP-N1 vector (Kasai *et al.*, 2008) was digested by *Xho*I and *Bam*HI and subcloned into the pNPY-Venus-N1 vector (Nagai *et al.*, 2002), which results in replacement of the NPY cDNA with a preproinsulin cDNA. The cDNA of the humanized monomeric KO1 were amplified from phmKO1-MN1 (MBL, Nagoya, Japan) using the following primers: 5′-CGGGATCCAATGGTGAGCGTGATCAAGCC-3′ and 5′-TTGCGGCCGCTCTAGATTAGGAGTGGGCCA-3′. The full-length KO1 cDNA inserted into the pGEM-T Easy (Promega, Madison, WI) was subcloned into the *Bam*HI and *Not*I sites of pNPY-Venus-N1 (pKO1-NPY-N1). All the cDNAs were sequenced using an automated DNA sequencer 3130*xl* (Applied Biosystems, Foster, CA). The recombinant adenovirus was generated as described previously (Yi *et al.*, 2002). The cDNA fragment cassette was ligated into the *Swa*I site of a pAxCAwt cosmid vector (Takara Bio, Otsu, Japan). MIN6 cells or pancreatic β cells were infected with adenoviruses at moi 10 for 2 d or otherwise under the indicated condition.

RNA interference

The recombinant adenoviruses encoding shRNAs were described previously (Lopes *et al.*, 2007). Briefly, they were constructed by inserting an inverted repeat of murine exophilin8-specific 21-nucleotide sequences (shRNA4–8) into pENTR/U6 (Invitrogen, Carlsbad, CA), which had been modified to carry an EGFP expression cassette. The ability of exophilin8 knockdown was assessed by real-time quantitative PCR. Briefly, total RNA of adenovious-infected MIN6 cells was reverse transcribed using Superscript First-Strand Synthesis System (Invitrogen). The following primer sets were used: GGAAGTGACTCCACGTTCTACA and CCTCGTTCTGTTTGTCCAGG for exophilin8, and GAAATCGTGCGTGACATCAAAG and TGTAGTTTCATGGATGCCACAG for β-actin, respectively. After incubation at 95°C for 30 s, the samples were incubated at 95°C for 3 s and 60°C for 20 s for 40 cycles. The DNA amplification was monitored by incorporation of SYBER Green (SYBR PremixEx Taq I; Takara Bio) on LightCycler 480 (Roche Applied Science, Mannheim, Germany). Exophilin8 mRNA levels were quantified by a delta–delta cycle threshold method.

Cell culture

The mouse insulinoma cell line MIN6 (Miyazaki *et al.*, 1990) was grown in high-glucose (25 mM) Dulbecco's modified Eagle's medium supplemented with 15% fetal calf serum (FCS) and 55 μM 2-mercaptoethanol and maintained in a humidified incubator with 95% air and 5% CO_2 at 37°C. A monolayer culture of pancreatic β cells was prepared as described previously (Kasai *et al.*, 2008). Briefly, isolated islets were hand-selected under a dissecting microscope and cultured overnight in RPMI-1640 medium (11 mM glucose) supplemented with 10% FCS, 100 U/ml penicillin, and 100 μg/ml streptomycin. They were then dissociated into single cells by incubation with trypsin-EDTA solution. The dispersed cells were cultured on poly-L-lysine (P6282; Sigma-Aldrich, St. Louis, MO)-coated cover glasses (round, 25 mm in diameter) in RPMI-1640 medium for 2 d. All animal experiments were performed according to the guidelines of the Animal Care and Experimentation Committee, Gunma University.

A batch insulin release assay

MIN6 cells were infected with adenoviruses encoding exophilin8-specific shRNAs. After 2 d, the cells were preincubated for 30 min in Krebs Ringer buffer (KRB; 15 mM HEPES, pH 7.4, 120 mM NaCl, 5 mM KCl, 2 mM $CaCl_2$, 1 mM $MgCl_2$, 12 mM $NaHCO_3$, 0.3% bovine serum albumin, and 2.8 mM glucose) and further incubated for 10 min in KRB or that containing 60 mM KCl. Insulin in the buffer and in the cells extracted with 0.1% Triton X-100 was measured in triplicate using an AlphaLISA insulin kit with EnVision 2101 Multilabel Reader (PerkinElmer, Waltham, MA).

Immunoblotting

HEK293 cells were transfected with an expression plasmid encoding EGFP- or mCherry-fused protein. The cells were lysed in 1 ml of a lysis buffer (20 mM HEPES, pH 7.5, 100 mM NaCl, 0.1% NP-40, 5 mM EDTA, 10 mM $MgCl_2$, and 1 mM dithiothreitol) for 10 min at 4°C. The cell lysates were centrifuged and the supernatants were incubated with either glutathione-*S*-transferase (GST)-fused protein immobilized on glutathione beads, or with rabbit polyclonal anti–red fluorescent protein antibody (MBL) followed by protein A Sepharose 4FF beads (GE Healthcare). The interacting

proteins were analyzed by immunoblotting with rabbit polyclonal anti-GFP antibody (MBL) at a 1:5000 dilution.

Immunostaining

MIN6 cells cultured on cover glasses were fixed with 3.7% formaldehyde in PBS for 30 min at room temperature. They were washed three times with PBS and then treated with 0.1% Triton X-100 in PBS for 30 min at room temperature. After blocking, the cells were incubated for 2 h at room temperature with guinea pig anti–porcine insulin serum (a gift from T. Matozaki and H. Kobayashi, Gunma University) at a 1:1000, rat monoclonal anti-HA antibody (clone 3F10; Roche Diagnostics, Mannheim, Germany) at a 1:1000 dilution, and mouse monoclonal antibodies toward Rab27a or EB1 (BD Biosciences, San Jose, CA) at a 1:100 dilution; or toward α-tubulin (clone B-5–1-2; Sigma-Aldrich) at a 1:2500 dilution. They were then incubated with the Alexa Fluor 488-, 555-, or 610-R-phycoerythrin–conjugated secondary antibody (Invitrogen) at a 1:500 dilution for 1 h at room temperature. For the F-actin labeling, fixed cells were incubated with rhodamine-conjugated phalloidin (Invitrogen) for 1 h at room temperature.

Confocal microscopy

Cell imaging was carried out on a Zeiss LSM 5 Pascal laser scanning confocal microscope (Carl Zeiss, Heidelberg, Germany). A 63× oil immersion objective lens with a 1.4 numerical aperture was used with the pinhole setting to Airy 1. EGFP-tagged probes and Alexa Fluor 488–conjugated secondary antibody were excited using a 488-nm argon–ion laser, and the emission light was collected at 505–530 nm. mCherry-tagged probes, Alexa Fluor 555–conjugated antibody, and rhodamine-conjugated phalloidin were excited using a 543-nm HeNe laser, and the light was collected at >560 nm. *Z* axial sections were collected at a 0.36-μm step through the cell, and the projected images were constructed using Zeiss LSM software (version 3.2 SP2). Images were processed using ImageJ (NIH, Bethesda, MD) and Adobe (San Jose, CA) Photoshop CS software.

FRAP was measured at a 3× zoom, with the confocal pinhole set to Airy 2.06. Bleaching was carried out using the FRAP macro on the Zeiss software. A square region of interest was bleached by maximal laser power. Fluorescence in the region was measured at 5-s intervals and then normalized. Ten prebleach and 40 postbleach frames were recorded per cell.

TIRF microscopy

TIRF microscopy was performed on an inverted microscope IX81 with an infinity-corrected, 100×/1.45 oil objective lens (Olympus, Tokyo, Japan). An incident light was introduced via a single-mode optical fiber and two illumination lenses (IX2-RFAEVA-2; Olympus). Venus- and EGFP-tagged probes were excited using a 488-nm argon ion laser. The laser beams were passed through an electromagnetically driven shutter A7419, which was opened synchronously with an electron multiplying charge-coupled device (EM-CCD) camera C9100–12 controlled by Aquacosmos software version 2.6 (Hamamatsu Photonics, Hamamatsu, Japan). Images were acquired every 82.9 ms. For simultaneous imaging of EGFP and Alexa Fluor 610-R-phycoerythrin fluorescence, a single 488-nm argon ion laser was used. An image splitter W-View with a 550 nm dichroic mirror (Hamamatsu Photonics) divided the red and green components, which were passed through 645AF75 and 510AF23 band pass filters (Chroma Technology, Bellows Falls, VT), respectively. The images were then projected side-by-side onto the EM-CCD camera.

TIRF microscopy for sequential imaging of EGFP and NPY-KO1 fluorescence was performed on an inverted microscope Eclipse with an Apo TIRF 100×/1.49 oil objective lens (Nikon, Tokyo, Japan). EGFP and KO1 were excited using 488- and 561-nm solid-state lasers, respectively. A dual-band filter set (LF488/561-A-000; Semrock, Rochester, NY) was applied on a light path. The images were acquired by the EM-CCD camera iXon DU-897 (Andor Technology, Belfast, Northern Ireland) controlled by NIS-element software (Nikon).

The image sequences acquired by TIRF microscopy were processed by a no neighbor deconvolution filter of the Aquacosmos software. The positions of insulin granules in an *x,y* plane parallel to the membrane glass interface were determined by their intensity and size using a quantification module provided by Volocity software version 5.3 (PerkinElmer). The mass centers of contiguous bright pixels were tracked over the sequence. The tracking data were filtered by its time span (at least 120 time points). For each insulin granule trajectory, the mean square displacement (MSD) in the *x,y* plane was calculated as described previously (Qian *et al.*, 1991). A plot of MSD as a function of time was linear and a two-dimension diffusion constant, D*x,y*, was derived from the slope of the curve (slope = 4 × D*x,y*). The relative *z* position of each granule from the interface was calculated from the fluorescence intensity as described previously (Johns *et al.*, 2001).

A single-cell insulin release assay was performed as described previously (Kasai *et al.*, 2008) with modifications. Briefly, MIN6 cells were infected with adenovirus encoding preproinsulin fused with Venus and further cultured for 2 d. To examine the effect of exophilin8 knockdown, MIN6 cells were doubly infected with adenovirus encoding NPY-KO1 and that encoding exophilin8 shRNA. TIRF microscopy was performed in an open chamber (Solent Scientific, Segensworth, UK) maintained at 35–37°C. The penetration depth of the evanescent field calculated from the device parameters was 100 nm. After preincubation for 30 min in KRB, the cells were stimulated with KRB containing 60 mM KCl for 5 min using an open perfusion microincubator (PDMI-2; Warner Instruments, Hamden, CT) and a Delta T Micro-Perfusion Pump (Bioptechs, Butler, PA). A fusion event with a flash was manually selected and assigned to one of two categories: "residents" that located in an evanescent field before fusion and "passengers" that were newly recruited from outside of an evanescent field and immediately fused to the plasma membrane. The average fluorescence intensity of individual vesicles was calculated in a 0.8 × 0.8-μm square placed over the vesicle center.

Measurement of the concentration of cytoplasmic free Ca^{2+}

MIN6 cells were loaded with 2 μM Fluo 4-AM (Dojindo, Kumamoto, Japan) for 30 min at 37°C in KRB and perfused on a PDMI-2 chamber. The imaging was carried out on an inverted microscope IX81 equipped with a CSU-X1 spinning disk confocal scanning unit (Yokogawa, Tokyo, Japan), a 488-nm solid state laser, and an EM-CCD camera (C9100–13; Hamamatsu Photonics). Fluo4 fluorescence was detected through a PlanApo N 60×/1.42 objective lens and analyzed using Aquacosmos software.

Statistical analysis

The significance of differences was assessed by a Mann–Whitney U test, or Kruskal–Wallis test followed by Dunn's test, using GraphPad Prism software (GraphPad Software, San Diego, CA).

ACKNOWLEDGMENTS

We thank A. Miyawaki (RIKEN Brain Science Institute) for providing the pNPY-Venus-N1 vector and S. Torii (Gunma University) for cloning of mouse exophilin8 cDNA. We also thank C. Samata,

K. Tomizawa, and S. Kanai for their technical support and J. Toshima and S. Kurose for their assistance in preparing the manuscript. This work was supported by grants in aid for scientific research and a grant of Global COE program from Ministry of Education, Culture, Sports, Science and Technology of Japan, and in part by grants from the Mitsubishi Foundation and from Novo Nordisk Insulin Study Award (to T.I.).

REFERENCES

Desnos C, Huet S, Fanget I, Chapuis C, Böttiger C, Racine V, Sibarita J-B, Henry J-P, Darchen F (2007). Myosin Va mediates docking of secretory granules at the plasma membrane. J Neurosci 27, 10636–10645.

Desnos C *et al.* (2003). Rab27A and its effector MyRIP link secretory granules to F-actin and control their motion towards release sites. J Cell Biol 163, 559–570.

El-Amraoui A, Schonn J-S, Küssel-Andermann P, Blanchard S, Desnos C, Henry J-P, Wolfrum U, Darchen F, Petit C (2002). MyRIP, a novel Rab effector, enables myosin VIIa recruitment to retinal melanosomes. EMBO Rep 3, 463–470.

Fukuda M, Kuroda TS (2002). Slac2-c (synaptotagmin-like protein homologue lacking C2 domains-c), a novel linker protein that interacts with Rab27, myosin Va/VIIa, and actin. J Biol Chem 277, 43096–43103.

Fukuda M, Kuroda TS, Mikoshiba K (2002). Slac2-a/melanophilin, the missing link between Rab27 and myosin Va: implications of a tripartite protein complex for melanosome transport. J Biol Chem 277, 12432–12436.

Gomi H, Mizutani S, Kasai K, Itohara S, Izumi T (2005). Granuphilin molecularly docks insulin granules to the fusion machinery. J Cell Biol 171, 99–109.

Handley MT, Burgoyne RD (2008). The Rab27 effector Rabphilin, unlike Granuphilin and Noc2, rapidly exchanges between secretory granules and cytosol in PC12 cells. Biochem Biophys Res Commun 373, 275–281.

Handley MT, Haynes LP, Burgoyne RD (2007). Differential dynamics of Rab3A and Rab27A on secretory granules. J Cell Sci 120, 973–984.

Honnappa S *et al.* (2009). An EB1-binding motif acts as a microtubule tip localization signal. Cell 138, 366–376.

Hume AN, Tarafder AK, Ramalho JS, Sviderskaya EV, Seabra MC (2006). A coiled-coil domain of melanophilin is essential for Myosin Va recruitment and melanosome transport in melanocytes. Mol Biol Cell 17, 4720–4735.

Izumi T (2007). Physiological roles of Rab27 effectors in regulated exocytosis. Endocr J 54, 649–657.

Izumi T, Kasai K, Gomi H (2007). Secretory vesicle docking to the plasma membrane: molecular mechanism and functional significance. Diabetes Obes Metab 9 (Suppl 2), 109–117.

Johns LM, Levitan ES, Shelden EA, Holz RW, Axelrod D (2001). Restriction of secretory granule motion near the plasma membrane of chromaffin cells. J Cell Biol 153, 177–190.

Kasai K, Fujita T, Gomi H, Izumi T (2008). Docking is not a prerequisite but a temporal constraint for fusion of secretory granules. Traffic 9, 1191–1203.

Lopes VS, Ramalho JS, Owen DM, Karl MO, Strauss O, Futter CE, Seabra MC (2007). The ternary Rab27a-Myrip-Myosin VIIa complex regulates melanosome motility in the retinal pigment epithelium. Traffic 5, 486–499.

Ménasché G, Ho C, Sanal O, Feldmann J, Tezcan I, Ersoy F, Houdusse A, Fischer A, de Saint Basile G (2003). Griscelli syndrome restricted to hypopigmentation results from a melanophilin defect (GS3) or a *MYO5A* F-exon deletion (GS1). J Clin Invest 112, 450–456.

Miyazaki J, Araki K, Yamato E, Ikegami H, Asano T, Shibasaki Y, Oka Y, Yamamura K (1990). Establishment of a pancreatic beta cell line that retains glucose-inducible insulin secretion: special reference to expression of glucose transporter isoforms. Endocrinology 127, 126–132.

Nagai T, Ibata K, Park ES, Kubota M, Mikoshiba K, Miyawaki A (2002). A variant of yellow fluorescent protein with fast and efficient maturation for cell-biological applications. Nat Biotechnol 20, 87–90.

Nagashima K, Torii S, Yi Z, Igarashi M, Okamoto K, Takeuchi T, Izumi T (2002). Melanophilin directly links Rab27a and myosin Va through its distinct coiled-coil regions. FEBS Lett 517, 233–238.

Noritake J, Watanabe T, Sato K, Wang S, Kaibuchi K (2005). IQGAP1: a key regulator of adhesion and migration. J Cell Sci 118, 2085–2092.

Qian H, Sheetz MP, Elson EL (1991). Single particle tracking: analysis of diffusion and flow in two-dimensional systems. Biophys J 60, 910–921.

Ramalho JS, Lopes VS, Tarafder AK, Seabra MC, Hume AN (2009). Myrip uses distinct domains in the cellular activation of myosin VA and myosin VIIA in melanosome transport. Pigment Cell Melanoma Res 22, 461–473.

Rudolf R, Kögel T, Kuznetsov SA, Salm T, Schlicker O, Hellwig A, Hammer III, JA, Gerdes H-H (2003). Myosin Va facilitates the distribution of secretory granules in the F-actin rich cortex of PC12 cells. J Cell Sci 116, 1339–1348.

Rudolf R, Salm T, Rustom A, Gerdes H-H (2001). Dynamics of immature secretory granules: role of cytoskeletal elements during transport, cortical restriction, and F-actin-dependent tethering. Mol Biol Cell 12, 1353–1365.

Slep KC, Rogers SL, Elliott SL, Ohkura H, Kolodziej PA, Vale RD (2005). Structural determinants for EB1-mediated recruitment of APC and spectraplakins to the microtubule plus end. J Cell Biol 168, 587–598.

Strom M, Hume AN, Tarafder AK, Barkagianni E, Seabra MC (2002). A family of Rab27-binding proteins: melanophilin links Rab27a and myosin Va function in melanosome transport. J Biol Chem 277, 25423–25430.

Thurmond DC, Gonelle-Gispert C, Furukawa M, Halban PA, Pessin JE (2003). Glucose-stimulated insulin secretion is coupled to the interaction of actin with the t-SNARE (target membrane soluble *N*-ethylmaleimide-sensitive factor attachment protein receptor protein) complex. Mol Endocrinol 17, 732–742.

Torii S, Takeuchi T, Nagamatsu S, Izumi T (2004). Rab27 effector granuphilin promotes the plasma membrane targeting of insulin granules via interaction with syntaxin 1a. J Biol Chem 279, 22532–22538.

Trifaró J-M, Gasman S, Gutiérrez LM (2008). Cytoskeletal control of vesicle transport and exocytosis in chromaffin cells. Acta Physiol 192, 165–172.

Trifaró J-M, Vitale ML (1993). Cytoskeleton dynamics during neurotransmitter release. Trends Neurosci 16, 466–472.

Varadi A, Ainscow EK, Allan VJ, Rutter GA (2002). Involvement of conventional kinesin in glucose-stimulated secretory granule movements and exocytosis in clonal pancreatic β-cells. J Cell Sci 115, 4177–4189.

Varadi A, Tsuboi T, Rutter GA (2005). Myosin Va transports dense core secretory vesicles in pancreatic MIN6 β-Cells. Mol Biol Cell 16, 2670–2680.

Waselle L, Coppola T, Fukuda M, Iezzi M, El-Amraoui A, Petit C, Regazzi R (2003). Involvement of the Rab27 binding protein Slac2c/MyRIP in insulin exocytosis. Mol Biol Cell 14, 4103–4113.

Wu X, Bowers B, Rao K, Wei Q, Hammer III, JA (1998). Visualization of melanosome dynamics within wild-type and dilute melanocytes suggests a paradigm for myosin V function in vivo. J Cell Biol 143, 1899–1918.

Wu XS, Rao K, Zhang H, Wang F, Sellers JR, Matesic LE, Copeland NG, Jenkins NA, Hammer III, JA (2002). Identification of an organelle receptor for myosin-Va. Nat Cell Biol 4, 271–278.

Wu XS, Tsan GL, Hammer JA III (2005). Melanophilin and myosin Va track the microtubule plus end on EB1. J Cell Biol 171, 201–207.

Yi Z, Yokota H, Torii S, Aoki T, Hosaka M, Zhao S, Takata K, Takeuchi T, Izumi T (2002). The Rab27a/granuphilin complex regulates the exocytosis of insulin-containing dense-core granules. Mol Cell Biol 22, 1858–1867.